SCIENCE CHINA
Earth Sciences

• RESEARCH PAPER •

September 2013 Vol.56 No.9: 1588–1598
doi: 10.1007/s11430-012-4571-4

Effect of opening the Drake Passage on the oceanic general circulation: A box model study

SHAO QiuLi[1], CHEN XianYao[1*] & HUANG RuiXin[2]

[1] *Key Laboratory of Data Analysis and Applications, State Oceanic Administration; The First Institute of Oceanography, State Oceanic Administration, Qingdao 266061, China;*
[2] *Woods Hole Oceanographic Institution, Woods Hole, MA 02543-1050, USA*

Received March 14, 2012; accepted June 25, 2012; published online January 15, 2013

The impacts of opening the Drake Passage (DP) on the oceanic general circulation are examined. When the DP is open, wind stress at mid- and high latitudes gives rise to a wind-driven gyre, which induces a meridional heat exchange between mid- and high latitudes in the Southern Ocean. After the opening of the DP, the Antarctic Circumpolar Current (ACC) forms and its associated strong temperature front blocks the heat transport from mid-latitudes to high latitudes. A simple box model is formulated, in which the effects of the wind stress (for the case of DP closed) and the thermal front (for the case of DP open) on the variability of Antarctic Bottom Water (AABW) and North Atlantic Deep Water (NADW) are explored. The sensitivity experiments demonstrate that: (1) When the DP is closed, the enhancement of the wind-driven gyre leads to the decline of AABW formation in the Southern Ocean and the increase of NADW formation in the North Atlantic. As a result, water in high latitudes of the Southern Ocean becomes warmer, so does the bottom water of global ocean. (2) When the DP is open, there is no formation of AABW until the intensity of thermal front along ACC exceeds a threshold value (it is 4.03°C in our model). Before the formation of AABW, temperature in most of the oceans is higher than that after the formation of AABW, which usually leads to the cooling of high latitudes of the Southern Hemisphere and the bottom water in global ocean. When the strength of the thermal front is lower than the critical value, there is no AABW formation, and temperature in most of the oceans is slightly higher. These results demonstrate that during the opening of the DP, changes in wind stress and the formation of the thermal front in the Southern Ocean can substantially affect the formation of AABW and NADW, thus changing the state of meridional overturning circulation in the global ocean.

Drake Passage, Antarctic Bottom Water, North Atlantic Deep Water, box model, wind stress, thermal front

Citation: Shao Q L, Chen X Y, Huang R X. Effect of opening the Drake Passage on the oceanic general circulation: A box model study. Science China: Earth Sciences, 2013, 56: 1588–1598, doi: 10.1007/s11430-012-4571-4

Changes in land-sea distribution and topography are among the most important factors inducing changes in ocean circulation [1]. Over the long geological history, major changes in ocean circulation and climate were usually accompanied by the changes of global topography; the opening of the DP was one of the most significant events in this category. According to paleogeographic record, the DP was opened up before late Eocene [2], which resulted in the formation of Antarctic Circumpolar Current (ACC), followed by the significant growth of ice sheet in Antarctica and rapid cooling of the deep ocean [3]. Berger's study [4] showed that the temperature difference between surface and bottom water in the equatorial area increased from 7°C before the opening of the DP to 26°C after the opening, representing the significant impacts of the opening of the DP on the global climate change. The fact is further confirmed by the other paleoclimatic observations [5].

*Corresponding author (email: chenxy@fio.org.cn)

Numerical simulations have demonstrated the important effect of DP opening on ocean circulation and global climate. Using an ocean circulation model with idealized topography, Gill and Bryan [6] found that the closure of the DP creates a condition favorable for the formation of AABW. However, when the DP is open, warm water from low latitudes cannot cross the ACC; thus, it sinks to the subsurface north of the DP and forms Antarctic Intermediate Water (AAIW). Meanwhile, an upwelling is generated in the south of the DP. Cox [7] and England [8] noted that the opening of the DP may change the overturning circulation in SH and induce the changes of water masses, such as AAIW. Taking the air-sea interaction into consideration, Toggweiler and Bjornsson [9] estimated that the sea surface temperature (SST) and air temperature (SAT) at high latitudes of the Southern Hemisphere (SH) could drop by 3°C after the DP opens, together with about the same amount of warming in high latitudes of the Northern Hemisphere (NH). Using a fully coupled model, Sijp and England [10] compared the states of global climate when the DP is closed, partly opened (with a channel depth of 690 m deep), and completely opened (with the realistic topography). They found that only when the DP is completely opened, NADW forms and leads to the warming of the NH and cooling of Antarctic Zone.

The comprehensive air-sea coupled models have their advantage to get better simulation of global ocean circulation; however, they rely heavily on parameterizations for subgrid scale processes. Unfortunately, these parameters are most tuned towards the current climate state. As a result, most models may not be able to simulate climate and oceanic circulation under climate conditions which are dramatically different from the current climate state. Compared with those complex models, box models [11] have some unique advantages because they require much less computer power; thus, they can be implemented for long time scale simulation. In addition, they can be used to explore the fundamental physical processes in the oceanic general circulation.

For example, they have been used in studies on the variability of thermohaline circulation [12, 13] and the formation of NADW [13, 14]. In this paper, we use a simple box model to explore the impacts of wind stress and ocean thermal front variability on the ocean circulation before and after the opening of the DP. Our box model incorporates both the Northern and Southern Hemispheres. In the NH, we will examine dynamical processes associated with the formation of NADW and its impacts in controlling THC. In order to simulate the effects of the DP on ocean circulation and climate change, the SH in the box model is divided into mid- and high-latitude columns, the latter corresponds to the area where AABW forms. In the vertical direction, there are three layers, and the second and third layers are designed for simulating the variation of NADW and AABW.

1 Model formulation and experiment design

1.1 Model formulation

In order to study Atlantic Meridional Overturning Circulation (AMOC), a 4×3 box model is formulated (Figure 1). Starting from the left hand side, the consequent columns represent the Antarctica, middle latitudes in the SH, the equatorial region (low latitudes) and middle and high latitudes in the NH. To ensure a stable state of AMOC [15], the low latitude (30°N–30°S) area in both hemispheres is com-

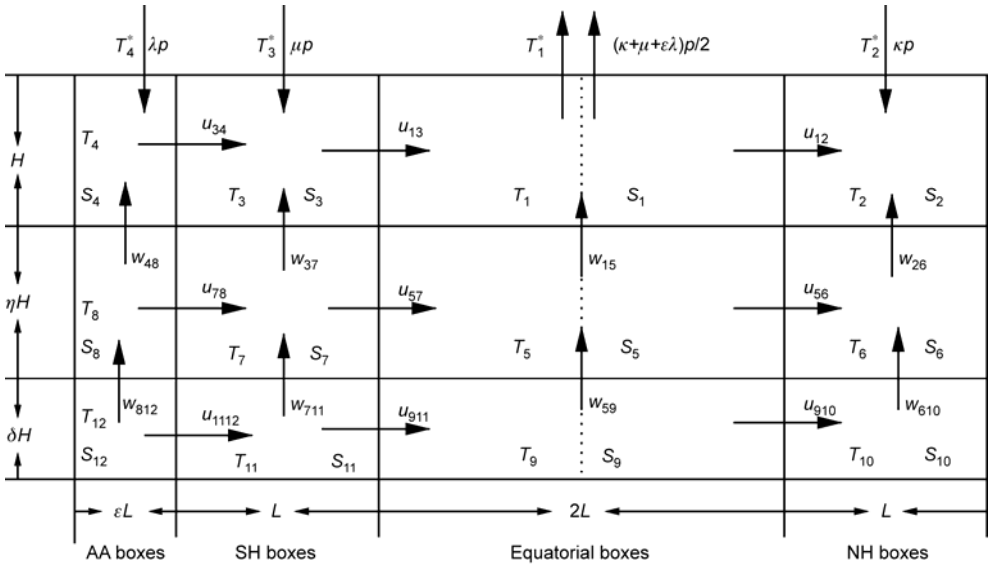

Figure 1 Sketch of the 4×3 box model in the Atlantic Ocean. T and S for temperature and salinity (with the subscripts indicating the relevant box numbers, starting the equatorial surface box as number one), u and w for the horizontal and vertical velocity, H and L for the depth and width, p for precipitation minus evaporation (freshwater flux), and T^* for specified reference temperature at the sea surface.

bined into a single water column. The middle latitude boxes in the Southern Hemisphere (hereafter SH boxes) span a range of 30°S to 60°S. To characterize the formation and variation of NADW the boxes representing middle and high latitudes in the Northern Hemisphere (hereafter NH boxes) range from 30°N to 60°N. To investigate the influence of the DP, we extend box models used in previous studies [12–14] by adding on a separate water column for the Antarctic Zone from the SH boxes, named Antarctica boxes (about 15° wide, hereafter AA boxes). There are two major branches in AMOC, and the upper one (related to NADW) and the lower one (related to AABW) are located at different depths [16]. In order to simulate such fundamental features, the model is divided into three layers in the vertical direction, with the thickness of 500, 1500 and 3000 m, respectively.

Similar to previous studies, we assume that the strength of THC is regulated by the meridional density difference between boxes at low and high latitudes, and all properties are well mixed in each box [11, 17]. Seawater density is assumed to be a linear function of salinity and temperature

$$\rho_i = \rho_0\left(1-\alpha T_i+\beta S_i\right),\ \ i=1,\ 2,\ 3,...,12, \tag{1}$$

where α=0.17 kg m^{-3} °C^{-1}, β=0.77 kg m^{-3} are the thermal expansion and haline contraction coefficients, respectively.

Pressure at any point in a water column can be calculated from hydrostatic relation. Because the model is highly truncated, the effect of Coriolis force is omitted. In the horizontal direction we assume that velocity is linearly proportional to the pressure gradient, that is $u=c\dfrac{\Delta p}{\Delta d}$, where c is a proportional coefficient, Δp is pressure difference between center points of two adjacent boxes, and Δd is distance between them.

After simple manipulations, the formula of velocity is derived. Take u_{12} as an example

$$u_{12}=-\frac{L}{3H}\kappa p-\frac{cgH}{9L}(2\Delta\rho_{12}+3\eta\Delta\rho_{56}+\delta\Delta\rho_{910}). \tag{2}$$

Introducing nondimensional parameters, $t=t'H/\Gamma$, $u_{ij}=u'_{ij}\cdot(L\Gamma)/H$, $w=\Gamma w'$, $p=\Gamma p'$, $T=T_0^*T'$, $S=S_0^*S'$, eq. (2) is reduced to

$$\begin{aligned}u_{12}=&-\frac{\kappa p}{3}+A_1\left[2\left(T_1-T_2\right)+3\eta\left(T_5-T_6\right)+\delta\left(T_9-T_{10}\right)\right]\\&-B_1\left[2\left(S_1-S_2\right)+3\eta\left(S_5-S_6\right)+\delta\left(S_9-S_{10}\right)\right],\end{aligned} \tag{3}$$

where $A_1=C_1\alpha T_0^*$, $B_1=C_1\beta S_0^*$, $C_1=\dfrac{cgH^2\rho_0}{9\Gamma L^2}$. T_0^* and S_0^* are reference temperature (25°C) and salinity (35). C_1 is the so-called frictional coefficient, which can be estimated from the vertical velocity of large-scale circulation in the world ocean [12] and it is assumed to be invariant under different climate conditions.

Other components of horizontal direction are slightly different, and yet they can be derived accordingly. The vertical velocities can be inferred from conservation of mass. Since density in the ocean varies very slightly, mass conservation can be approximately replaced by volume conservation; therefore, vertical velocity can be calculated from the divergence of horizontal velocity.

The upper boundary conditions are as follows:

(i) Temperature. A restoring boundary condition (Rayleigh condition) applies to the temperature of the upper layer

$$H_f=\rho_0 c_p\Gamma(T^*-T), \tag{4}$$

where $\Gamma\simeq 8.1\times10^{-6}$ m s^{-1} [18], T^* is the prescribed reference temperature on the surface. For simplicity, we set $T_1^*=T_0^*=25$°C, $T_3^*=T_2^*=0$. For the Antarctica, we set $T_4^*=-2$°C.

(ii) Salinity. A natural boundary condition applies, i.e., the freshwater flux through the upper surface of the upper-layer box is specified. For the steady state, the algebraic sum of the applied fresh water fluxes is zero.

Taking box 1 as an example, the equations for the heat and salt balances are

$$\begin{aligned}2\rho_0 c_p HL^2\frac{\mathrm{d}T_1}{\mathrm{d}t}=&\rho_0 c_p HL\left(u_{13}T_3-u_{12}T_1\right)\\&+2\rho_0 c_p L^2 w_{15}T_5+2\rho_0 c_p L^2\Gamma(T_1^*-T_1),\end{aligned} \tag{5}$$

$$2\rho_0 c_p HL^2\frac{\mathrm{d}S_1}{\mathrm{d}t}=\rho_0 c_p HL\left(u_{13}S_3-u_{12}S_1\right)+2\rho_0 c_p L^2 w_{15}S_5. \tag{6}$$

Introducing the non-dimensional variables, the corresponding equations become

$$\frac{\mathrm{d}T_1}{\mathrm{d}t}=0.5\left(u_{13}T_3-u_{12}T_1\right)+w_{15}T_5+1-T_1, \tag{7}$$

$$\frac{\mathrm{d}S_1}{\mathrm{d}t}=0.5\left(u_{13}S_3-u_{12}S_1\right)+w_{15}S_5. \tag{8}$$

Similarly, a whole set of equations of temperate, salinity and velocity for all boxes can be obtained. Some parameters of the box model are shown in Table 1.

1.2 Design of experiments

The oceanic circulation and atmospheric circulation have been significantly changed after the opening of the DP, including the abrupt reversal in THC [19, 20], from the Southern Ocean Deep Water (SODW) dominated mode to the NADW dominated mode [20]. This thermohaline reversal is a complex process, including many changes in the

Table 1 Parameters used in the model

Parameter	Value	Remarks
L	3×10^6 m	width
H	500 m	depth of upper layer
η	3	coefficient of the depth of middle layer
δ	6	coefficient of the depth of bottom layer
ε	0.5	coefficient of the width of Antarctica column
λ	1	
μ	1	
κ	1	
p	$0.3\times3.8\times10^{-8}$ m s^{-1}	mean annual precipitation [12]
C_1	200/9	frictional coefficient

climate coupled system, such as changes in bathymetry and air-sea interaction (such as wind stress, heat flux, and evaporation and precipitation). If changes in the distribution of evaporation and precipitation were taken into consideration, reversal of thermohaline circulation can be simulated in our box model as well. However, our focus in this study is the effect of wind stress changes associated with the closure of the DP and thermal fronts associated with an opened DP on formation and change of NADW and AABW. Therefore, we designed the following experiments:

First, appropriate initial conditions are chosen, and the model is run until a steady state of thermodynamic-mode circulation is reached (a thermodynamic-mode circulation is controlled by buoyancy fluxes alone, including heat flux and freshwater). This steady model circulation is further integrated forward in time by adding wind-driven gyration between boxes 1 and 2 and between boxes 1 and 3, which represents a simple parameterization of the dynamic effect of wind stress. When the model reaches a steady state again, we use it as a testing bed for further numerical experiments. Such a circulation can be called a thermodynamic-dynamic mode.

There are two sets of experiments. The first set is designed for the case of a closed DP. In this set, wind stress in the SH and Antarctic boxes is changed, i.e., the strength of the gyration between SH and AA boxes is alternated. The second set is designed for the case of an opened DP. In this set, the temperature gradient, i.e., the strength of thermal front, between the two columns is changed. By comparing variability of temperature, salinity and volume transport obtained from these two sets of experiments, we can explore the impacts of closing/opening the DP.

1.2.1 The initial state

The initial state of model is obtained by two steps, as described above.

(i) A thermodynamic-mode circulation controlled by buoyancy fluxed alone

Due to different choices of parameters, there are two major modes of THC in box models [12]. The thermal mode refers to the circulation in which the water in equatorial region warms up and spreads poleward at the surface, cooling all the way and thus sinking in the high latitudes; finally, water returns to the equator via deep flow. The saline mode flows in an opposite direction. Observations indicate that the circulation in the Atlantic Ocean is in thermal mode [12, 21]; thus, we choose appropriate salinities and temperatures to obtain a representative thermal mode controlled by buoyancy fluxes, in which cold water upwellings in low latitudes, and there are formations of NADW and AABW in the Northern and Southern Hemispheres, respectively.

Using the initial conditions of Table 2, we run the model to a steady state, named as initial state 1, whose temperatures and salinities are shown in Table 3. Since the model is subject to surface buoyancy forces only, the circulation is called in a thermodynamic mode.

(ii) The final initial state including wind-stress induced gyration

To introduce the impacts of wind stress to the steady state obtained in a), the parameterization scheme of Guan and Huang [22] is employed, i.e., the impacts of wind stress are represented by horizontal volume exchange rate, gyration ω between adjacent boxes in the upper ocean.

Based on the NCEP data, the zonally integrated Ekman transport induced by wind stress is 9 Sv at the latitude of the DP in the Atlantic sector [23]. For simplicity, we assume that when the DP is open, the strength of gyration between boxes 1 and 2 is ω_{12}=9 Sv, and that between boxes 1 and 3 is ω_{13}=9 Sv, while that between boxes 3 and 4 is set to 0.

Table 2 Initial conditions for each box

Box number	1	2	3	4	5	6	7	8	9	10	11	12
Temperature (°C)	25	2.5	2.5	–2.5	2.5	2.5	2.5	–2.5	2.5	2.5	2.5	–2.5
Salinity (psu)	35	35	35	35	35	35	35	35	35	35	35	35

Table 3 A steady state controlled by buoyancy fluxes alone

Box number	1	2	3	4	5	6	7	8	9	10	11	12
Temperature (°C)	22.59	1.47	2.88	–1.04	0.23	1.47	0.42	–1.04	–1.04	–0.92	–1.04	–1.04
Salinity (psu)	35.53	34.82	35.19	34.98	34.96	34.82	35.06	34.98	34.98	34.98	34.98	34.98

Table 4 Steady state controlled by both buoyancy flux and wind stress

Box number	1	2	3	4	5	6	7	8	9	10	11	12
Temperature (°C)	20.96	3.20	4.28	–0.77	0.76	3.20	0.30	–0.77	–0.77	–0.83	–0.77	–0.77
Salinity (psu)	35.35	35.07	35.16	34.95	35.00	35.07	35.00	34.95	34.95	34.98	34.95	34.95

With the gyration ω, which is induced by wind stress described above, added on to the steady state obtained in a), we obtain another steady state as the basis of sensitivity experiments, and the corresponding temperatures and salinities are shown in Table 4. This steady state is also a stable thermal-mode circulation, in which the transport of NADW and AABW is 4.25 Sv and 6.64 Sv, respectively. The temperature difference between box 3 and box 4 is 5.04°C. Since the model is now subject to both buoyancy force and wind stress, the circulation is called in a thermodynamic-dynamic mode.

1.2.2 Experiment I—the impacts of wind stress

Stommel [11] assumed the THC is driven by buoyancy, without taking the impacts of wind stress into consideration [22]; therefore, his model could not be used to study the impacts of wind stress at the latitude of the DP. Based on paleoclimatic proxy data, Toggweiler and Samuels [24, 25] pointed out that the wind stress at the DP, instead of buoyancy, plays a crucial role in driving THC. There is no east-west boundary at the latitude of the DP; thus, the Sverdrup theory does not apply. As a result, water mass transport across this latitude band consists of non-geostrophic flow only, and such transport can be merely driven by wind stress only. Under certain assumptions, the strength of AMOC can be fully expressed as a function of wind stress at the DP [26].

To investigate the impacts of wind stress, the experiment is designed as follows. Starting from the steady state described in Table 4, we keep surface buoyancy forcing on unchanged, and vary the strength of gyration between boxes 3 and 4 ω_{34}, whose value is set to the following values: 0, 4.5, 9, 18, 27, 36, 45 Sv. For each value of ω_{34}, the model is restarted from the same initial state and run to a steady state. Through this process, we can examine the transient (namely, the time-dependent) behavior of the system in response to changes in the strength of wind stress.

1.2.3 Experiment II—the impacts of the thermal front

The opening of the DP leads to the formation of ACC, and thus exerts a profound influence on global climate [10, 27]. According to the thermal wind relation $\boldsymbol{f}\cdot\nabla\vec{V}=(g/\rho_0)\nabla\rho$, the vertical shear of zonal horizontal velocity is linked to the meridional density gradient. Taking the volume transport of ACC as 130 Sv [27] and omitting the contribution due to salinity, the temperature difference between boxes 3 and 4 is estimated at 6°C (This calculation is based on the assumption that density is a linear function of temperature and salinity).

In our model, due to the wind-stress induced gyration, temperature and salinity can exchange freely between boxes 3 and 4 when the DP is nominally closed. After the DP is opened, a strong thermal front is formed, which blocks such exchange. We designed the following experiments to study this dynamic effect. Restarting from the initial state and keeping the other boundary conditions unchanged, we run the model replacing the restoring boundary condition of T_4^* for box 4 by the following condition. In this experiment T_4^* is no longer prescribed as a constant; instead, it can change with temperature of box 3 $T_4^*=T_3-\Delta t_{34}$, where Δt_{34} is prescribed, and its value can be set to the following values: 0, 1, 2, 3, 4, 5, 6, 7°C.

2 Model results

2.1 The impacts of wind-stress induced gyration

2.1.1 Changing of the wind-induced volume transport ω_{34}

As described above in Experiment I, ω_{34} represents the role of wind stress in the latitude band of the DP. With the increase of ω_{34}, the temperatures of all boxes increase, except for box 1. In comparison, the largest temperature increase is found in the bottom layer, especially in box 10, whose temperature increases by 2.7°C. Changes of temperature and salinity of boxes 1–4 induced by change of ω_{34} are shown in Figure 2. Because the relaxation temperature is specified in upper layer, temperature change in equatorial upper layer box 1 is minimal, with the amplitude only of 0.015°C. The largest temperature changes occur in boxes 3 and 4, reaching about 1.1°C and 1.8°C, respectively. Obviously, the wind-induced gyration has a much bigger impact on temperature and salinity for the boxes directly exposed to surface than the other boxes. The temperature difference of box 1 and box 9 shows a decrease trend, which is consistent with the discovery inferred from paleoceanography record that the temperature difference between the equatorial surface and bottom layers was much smaller than that in the present climate [4].

Toggweiler and Bjornsson [9] pointed out that heat transfer of THC linked to the DP is set up primarily by the circulation at high latitudes of the SH and the NH, and changes in the temperature at the equatorial band play a minor role only. In our model, however, temperature is slightly reduced at the equatorial band, and synchronous warming in high latitudes of both the Southern and Northern Hemispheres is observed. Such changes can be attributed to the following reasons. (1) Increase of the wind-stress induced gyration results in more heat being transferred

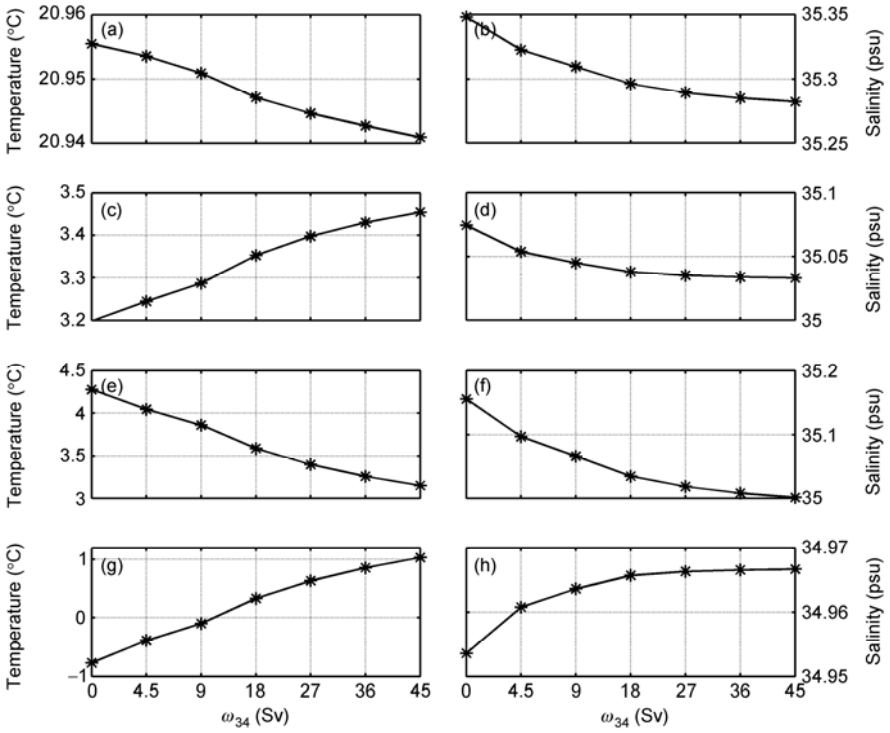

Figure 2 Dependence on ω_{34} of temperature and salinity in upper layer boxes. Temperatures of boxes 1–4 are shown in the left panels, salinities on the right. The stars mark the experimental values whereas the lines clearly show the trend.

from the SH boxes to the AA boxes, giving rise to the cooling of the equatorial region. Meanwhile, the gyration between boxes 1 and 2 leads to warming in the Northern Hemisphere boxes. (2) There is a slight increase of upwelling at the equatorial band, which brings cold deep water to the upper layer, leading to the cooling of the surface temperature.

Changes in salinity are relatively small. This may be because salinities we set are uniform at the initial state. As ω_{34} is increased, the salinities of all boxes in middle and bottom layers are slightly decreased, except for boxes 4 and 8. Given the thermal expansion coefficient and the haline contraction coefficient and the range of temperature and salinity, we can find that temperature plays a more important role than salinity does. This finding is consistent with the results obtained by Sijp and England [28] through numerical experiments based on a coupled model. Once bottom water is formed in the AA boxes, boxes 4, 8, and 9–12 have the same temperature and salinity. This implies that AABW is formed and it is transported northward, which will be discussed further shortly.

The ranges of velocity change decrease gradually from top to bottom (figure not shown), so does volume transport. Changes of major water masses are shown in Figure 3. According to our model design, AABW is represented by downwelling in AA boxes (with specific reference to that from box 4 to box 8). The formation of AABW changes slightly when ω_{34} changes from 0 to 4.5 Sv and further to 9 Sv. However, once it reaches the same value of 9 Sv as the other two gyrations, the decreasing speeds up. The formation of AABW is reduced to 6 Sv when ω_{34} is 45 Sv, and such a large decline results from temperature rising in AA boxes due to large ω_{34}. AABW with high temperature and low salinity is the main source of bottom water in the world ocean. It flows northward along the ocean floor, and its trace can be found in 50°N [16]. In our box model, the

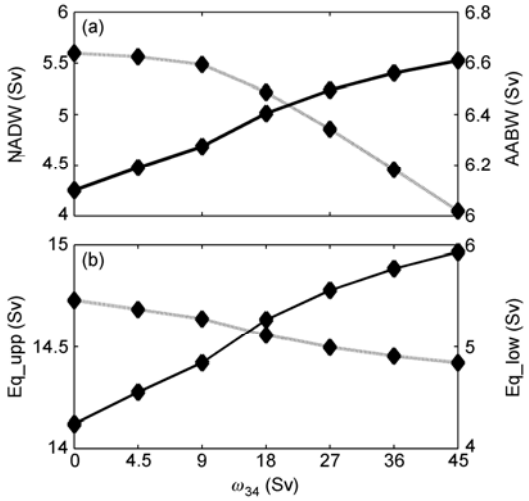

Figure 3 Dependence of the volume fluxes of the major water masses on ω_{34}. (a) The solid line for NADW and the dashed line for AABW. (b) Equatorial upwelling, the solid line for the upper layer, and the dashed line for the lower layer. In both panels, the values in experiment are marked in diamonds.

properties of AABW can be traced to box 9, that is, around 30°N, which is consistent with observations. With the increase of ω_{34}, AABW formation is weakened so that less bottom water reaches the latitudes north of 30°N, and this explains why we obtain the maximal amplitude of change in box 10. In contrast to the trend of the volume transport of AABW, the volume transport of NADW (denoted by sinking from box 2 to box 6) gradually increases. This is related to the so-called see-saw effect [9, 10] of the high-latitude temperatures between both hemispheres. During this period, the upwelling of upper layer in low latitudes shows an increasing trend (which is the reason for temperature decrease of box 1), whereas that of lower layer decreases.

2.1.2 Transient responses of the initial state to the wind-stress induced gyration

In this section, we examine the transient behaviors of the system to the addition of a gyration of ω_{34} = 9 Sv. Overall, ranges of temperature changes for boxes in the NH and the Antarctic zone are significantly higher than those of other regions in the same layer. The largest adjustment appears still in box 10, which is approximately 1°C. As for salinity, the ranges of changes decrease gradually from top to bottom. Adjustment of salinity in the bottom layer takes longer time, which is in agreement with Oliver et al. [17]. Huang et al. [12] suggested that thermohaline catastrophe is a surface phenomenon. However, there is no such catastrophe in our experiment; in fact, the adjustment in our model experiments takes place along a different path. Although changes of properties first take place in the surface layer, the signal can penetrate to deep boxes. In particular, the temperature adjustment can be transferred downward rapidly. As a result, the whole circulation system changes accordingly.

Figure 4 shows the time evolution of temperature and salinity of boxes 1–4 and 8, and the formation rates of NADW and AABW. As mentioned above, gyration has much greater impact on the boxes it directly affects. Therefore, adjustments of boxes 3 and 4 are nearly complete shortly after the gyration perturbations set in, and the corresponding amplitudes of change are larger than other boxes (Figures 4(c) and 4(d)). As the major factors controlling the formation of AABW, the adjustment of temperature and salinity in box 8 is crucial in determining the circulation of whole basin, in particular in the deep ocean. Since ω_{34} is directly applied to box 4, it warms box 4, and thus more heat is transferred to box 8. Salinity in box 8 increases during the first phase of adjustment (Figure 4(e)). In comparison, density perturba-

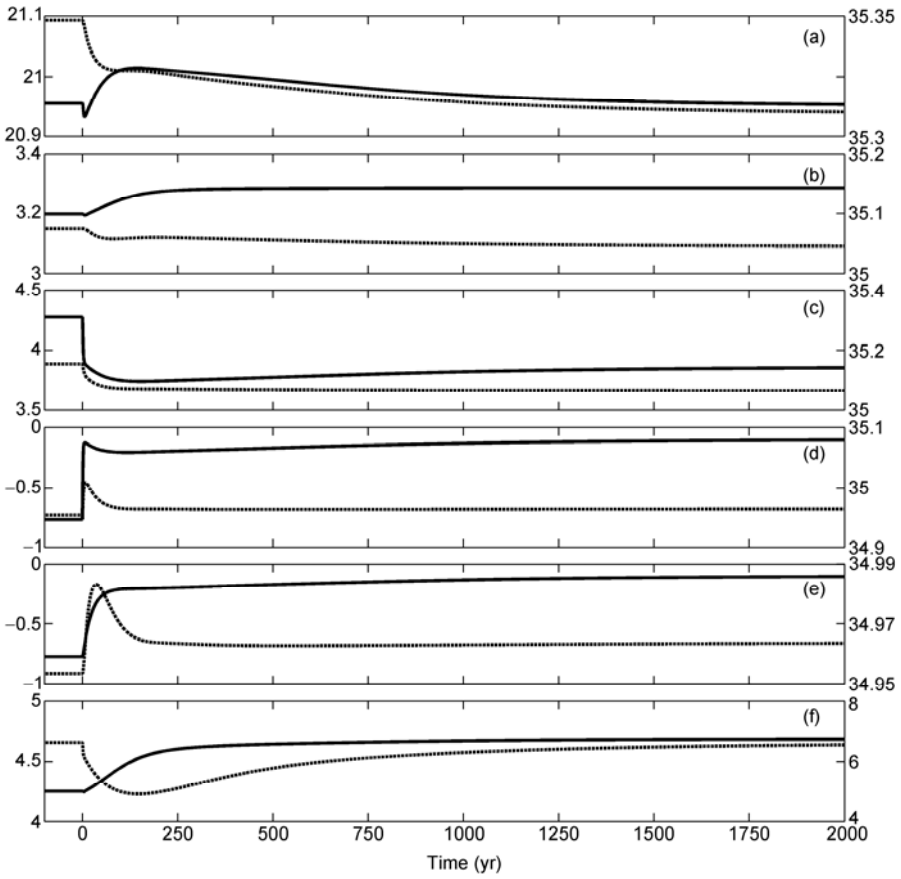

Figure 4 Time evolution of some model properties for the case in which perturbation of ω_{34} is 9 Sv. (a)–(e) Temperatures (solid line in unit of °C) and salinities (dashed line) of boxes 1–4 and 8; (f) the formation rates of NADW (solid line) and AABW (dashed line). To be clear, evolution of these properties is drawn from the time when the perturbations set in.

tion due to temperature increase overpowers that due to salinity change during this stage. As a result, the formation rate of AABW decreases due to warming of box 8. As time progressing, the formation rate of AABW enters the recovery phase. When the model runs to 2000 yr, both positive salt feedback and negative thermal feedback come to a new equilibrium stage. Their combined effects maintain the formation rate of AABW at a level slightly lower than the initial value.

The formation rate of NADW is increased and has a shorter adjustment time than AABW. Salinity adjustment in boxes 1 and 2 is quite different from that in box 8. In fact, salinity adjustment in boxes 1 and 2 takes much longer time and has almost the same tendency (Figures 4(a) and 4(b)). However, as the formation of NADW is controlled primarily by temperature rather than salinity, and the adjustment of temperature difference is established in less than 250 yr from the beginning. Consequently, the adjustment of NADW formation takes much less time than AABW. The difference in adjustment time of NADW and AABW is closely related to changes of the deep/bottom water circulation. The typical time scale for the global thermohaline circulation is on the order of a thousand years; thus, the adjustment of AABW takes much longer time [29].

2.2 The impacts of the thermal front

2.2.1 Changing of the strength of thermal front

The formation of the thermal front due to the opening of the DP has a significant impact on THC. The strength of this front plays a key role in regulating the circulation. When $\Delta t_{34} \leqslant 4$°C (especially when $\Delta t_{34} \leqslant 3$°C), temperatures in all boxes change only slightly. For each fixed value of Δt_{34}, boxes in the middle layer (boxes 5–8) have the same temperature, because there is no AABW formation and NADW plays a dominated role. As can be seen from Figure 5, there is a decreasing trend of temperature of the upper layer boxes, but the tendency is not remarkable, except in box 4. When Δt_{34} increases, temperature in box 4 decreases rapidly. It can even drop below 0°C when $\Delta t_{34} = 4$°C, which greatly benefits the formation of AABW. Temperatures in deep layer boxes tend to increase, but the amplitude of change is less than 0.2°C. The largest temperature adjustment appears when Δt_{34} is increased from 4 to 5°C. All properties have a linear trend when $\Delta t_{34} \geqslant 5$°C.

Change of salinity is more subtle than that of temperature. This can be attributed to the fact that the restoring boundary condition for temperature is employed in this experiment, whereas salinity has only passive responses accordingly [30]. Similarly, the largest changes of salinity appear when Δt_{34} is increased from 4 to 5°C. The largest salinity change appears in box 4 and salinity change in box 3 is slightly smaller. Obviously, changes of the thermal front also affect its neighboring ocean region the most.

As discussed above, when $\Delta t_{34} \leqslant 4$°C there is no AABW formation and NADW plays a dominating role. In

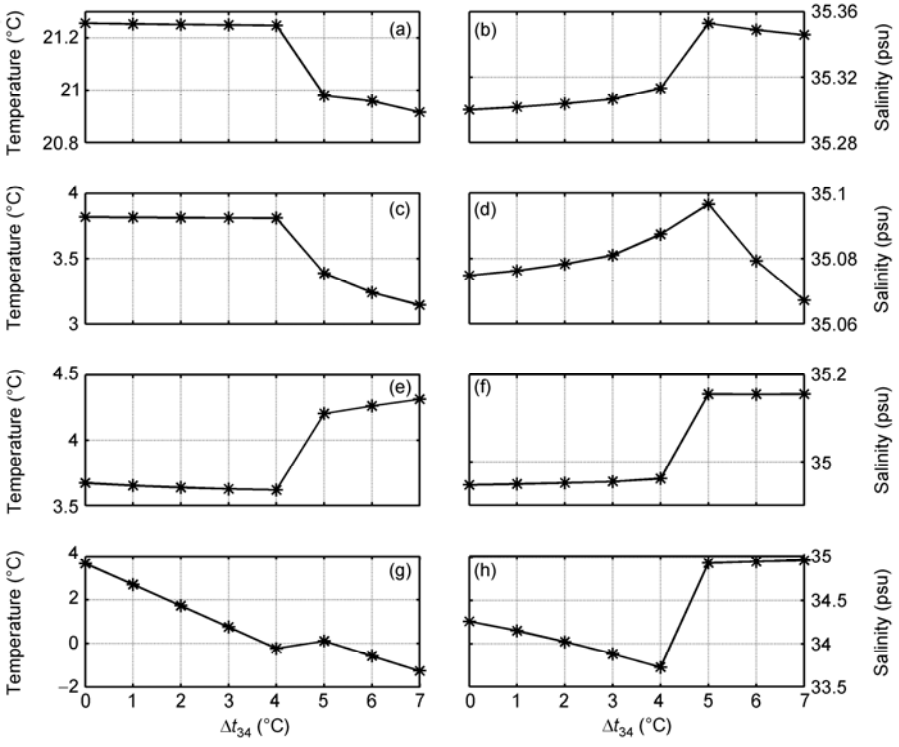

Figure 5 Same as in Figure 2, but for Δt_{34} changing.

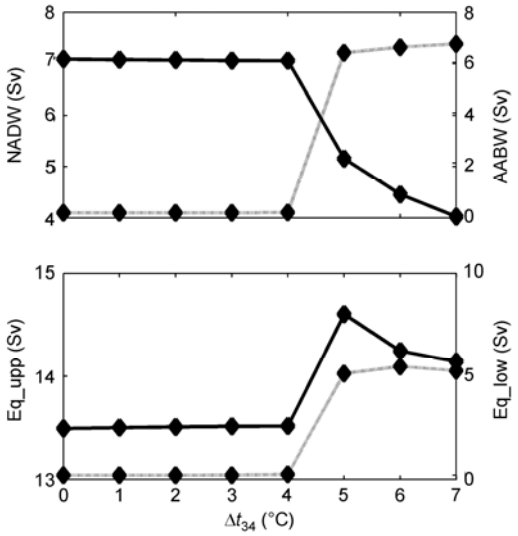

Figure 6 Same as in Figure 3, but for Δt_{34} changing.

this case, NADW can even extend to the Antarctic Zone, and thus temperature in boxes 5–8 is the same. No significant changes of formation of NADW and upwelling at low latitudes are detected when $\Delta t_{34} \leqslant 4$°C. When Δt_{34} is increased further, the system goes through an abrupt change (Figure 6). AABW begins to form, and its rate increases from 0 to 6.5 Sv. In contrast, the formation rate of NADW suddenly decreases from 7.2 to 5.4 Sv. Changes of NADW and AABW tend to be slow when $\Delta t_{34} \geqslant 5$°C. These results show that there is a threshold in the response of the system to increase of the strength of the thermal front. In our model, the value is 4.03°C. For any given value of $\Delta t_{34} \geqslant 5$°C, water in the column of AA region and in the bottom layer south of the equatorial region has the same temperature, whereas temperatures of the middle layer decrease gradually from north to south. This suggests that after the formation of AABW, the controlling power of NADW is reduced. In contrast to the response to gyration, when Δt_{34} is increased from 4 to 7°C, change in upwelling at low latitudes is not monotonic, which may result from the mutual adjustments of NADW and AABW, plus the adjustments of temperature and salinity in the equatorial band.

2.2.2 Transient responses of the initial state to thermal front perturbation

In the stable initial state, temperature of box 3 is 2.88, and thus Δt_{34} is 4.88°C. In the previous section, we showed that there is a rapid response of the system when Δt_{34} excesses 4.03°C. In other words, the adjustment processes are different for $\Delta t_{34} = 4$°C and $\Delta t_{34} = 5$°C. These two processes are examined below.

The time evolution of the model for the case $\Delta t_{34} = 4$°C is shown in Figure 7 (solid lines). The temperature changes in boxes of the upper and middle layers in SH and AA region have amplitudes larger than other boxes of the same layer, and change in box 8 is the largest (4.3°C). In the bottom layer, the largest change in temperature still appears at the northern end of the model (box 10). The amplitudes of salinity decrease gradually from the top to bottom, with the maximum appearing in box 4, being 1.7 psu. Because we choose to parameterize the strength of the thermal front by specifying $T_4^* = T_3 - \Delta t_{34}$, temperature in box 4 raises drastically right after the perturbation set in (see Figure 7(d)). Temperature adjustment of boxes 3 and 4 can induce changes in the circulation, and thus salinity changes in response. Afterward, salinity in box 4 begins to decline, and its trend is similar but slightly lags behind the temperature. The abrupt warming of box 4 at the beginning of the experiment results in temperature rising in most areas in the model during the first phase of adjustment, when NADW is dominating. The anomalous heat collected from the upper layer of the equatorial region and the NH is transported to the AA region by NADW; hence, temperature of the middle and bottom layer over there is increased, which in turn leads to the decrease of AABW formation.

When t_{34}=5°C, properties changes in the model ocean are smaller than the case t_{34}=4°C. The circulation pattern in this case is similar to that for the case with horizontal volume exchange ω_{34} added on. Temperature changes in all boxes are similar to those described in Section 2.1. However, the adjustment of salinity behaves differently. Noting that adjustments of NADW and AABW are similar to those induced by changing the strength of the wind-stress induced gyration. Therefore, the circulation is thermally controlled. Comparing these two cases, Δt_{34}=4°C and Δt_{34}=5°C, we conclude that in the case of front induced circulation change, e.g., Δt_{34}=4°C, the adjustment of the system is relatively fast. As a result, the model ocean goes through an immediate and remarkable adjustment.

3 Summary and conclusions

In this study we examine the influence of opening the DP on the general circulation using a simple box model. Two sets of experiments are designed to test the impacts of the wind-stress induced gyration and the thermal front at the latitude band of the DP on the circulation for the cases with the DP closed or open.

When the DP is closed and the strength of gyration at the latitude band of the DP is increased, the formation of NADW is enhanced but the formation of AABW declines. When gyration is greater than 4.5 Sv, AABW can even reach north of 30°N and exerts a controlling effect on bottom water of the whole model ocean. Waters in the AA boxes and bottom layer warm up, and temperature difference decreases between the upper and bottom layers at low

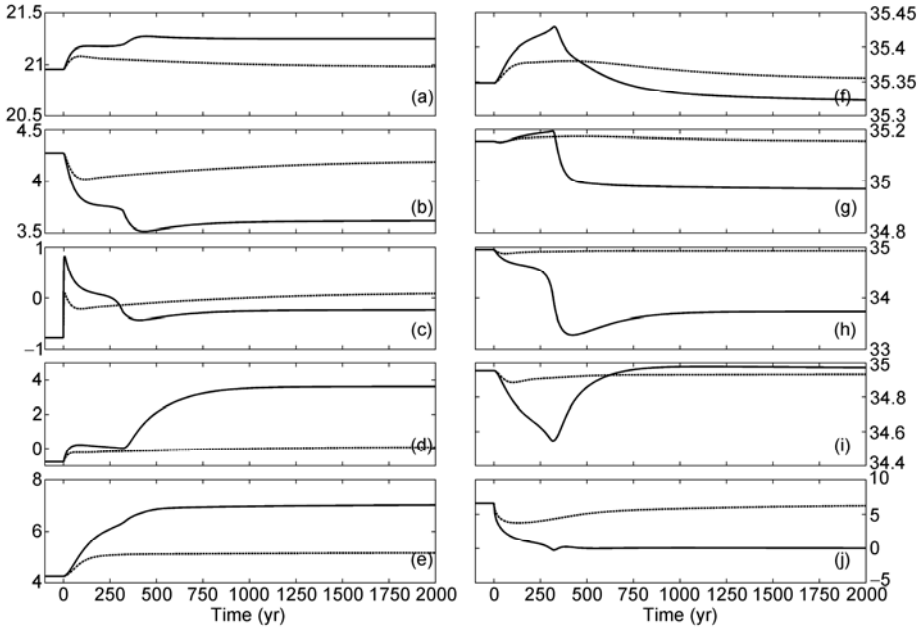

Figure 7 Time evolution of some model properties for cases t_{34}=4°C (solid lines) and t_{34}=5°C (dashed lines). (a)–(d) Temperatures (°C) of boxes 1, 3, 4 and 8 and the conresponding salinities (psu); (e) and (j) formation rates of NADW and AABW. T=0 indicates the beginning of these experiments when the perturbations set in.

latitudes. Both facts imply that the opening of the DP can lead to the cooling of subsurface ocean.

One of the key findings of our model is the remarkable effect of the thermal front formed after the opening of the DP on THC. When the thermal front is weaker or stronger than a critical value, the circulation is significantly different. Below this critical value a major feature is no AABW formation, while NADW plays a dominate role in controlling the temperature. When the thermal front becomes stronger than the critical value, through a rapid process AABW begins to form. Afterward, AABW, instead of NADW, begins to play a leading role. Our model results show that the changes of wind stress and the formation of thermal front during the course of the DP opening and ACC widening affect the formation of NADW and AABW, and further change the state of THC.

The model presented here is highly truncated, without including many important processes, such as evaporation/precipitation, sea-air interaction, and sea ice. These physical mechanisms are, however, indispensable for a comprehensive study of the mode shift of THC; thus, they should be taken into consideration in future study.

We express our sincere gratitude to the members of Key Laboratory of Data Analysis and Applications, SOA, who help greatly in this work. We thank anonymous reviewers for their constructive comments. This work was supported by National Basic Research Program of China (Grant No. 2012CB957802), the Chinese Polar Environment Comprehensive Investigation & Assessment Programmes (Grant No. CHINARE2012-04-04), Program of International Science and Technology Cooperation (Grant No. S2011GR0348),and National Natural Science Foundation of China (Grant No. 41176029).

1 Nong G T, Najjar R G, Seidov D, et al. Simulation of ocean temperature change due to the opening of Drake Passage. Geophys Res Lett, 2000, 27: 2689–2692
2 Scher H D, Martin E E. Timing and climatic consequences of the opening of Drake Passage. Science, 2006, 312: 428–430
3 Kennett J P. Cenozoic evolution of Antarctic glaciation, the circum-Antarctic Ocean, and their impact on global paleoceanography. J Geophys Res, 1977, 82: 3843–3860
4 Berger W H. Paleoceanography: The deep-sea record. In: Emiliani C, ed. The Sea. New York: Wiley-Interscience, 1981. 1437–1519
5 Zachos J, Pagani M, Sloan L, et al. Trends, rhythms, and aberrations in global climate 65 Ma to present. Science, 2001, 292: 686–693
6 Gill A E, Bryan K. Effects of geometry on the circulation of a three dimensional southern-hemisphere ocean model. Deep-Sea Res, 1971, 18: 685–721
7 Cox M D. An idealized model of the world ocean. Part I: The global-scale water masses. J Phys Oceanogr, 1989, 19: 1730–1752
8 England M H. On the formation of Antarctic intermediate and bottom water in ocean general circulation models. J Phys Oceanogr, 1992, 22: 918–926
9 Toggweiler J R, Bjornsson H. Drake Passage and palaeoclimate. J Quaternary Sci, 2000, 15: 319–328
10 Sijp W P, England M H. Effect of the Drake Passage throughflow on global climate. J Phys Oceanogr, 2004, 34: 1254–1266
11 Stommel H M. Thermohaline convection with two stable regimes of flow. Tellus, 1961, 13: 224–230
12 Huang R X, Luyten J R, Stommel H M. Multiple equilibrium states in combined thermal and saline circulation. J Phys Oceanogr, 1992, 22: 231–246
13 Lohmann G, Gerdes R, Chen D. Stability of the thermohaline circulation in a simple coupled model. Tellus A, 1996, 48: 465–476
14 Stastna M, Peltier W R. On box models of the North Atlantic thermohaline circulation: Intrinsic and extrinsic millennial timescale variability in response to deterministic and stochastic forcing. J Geophys Res, 2007, 112: C10023
15 Marotzke J, Welander P, Willebrand J. Instability and multiple steady states in a meridional-plane model of the thermohaline circulation. Tellus A, 1988, 40: 162–172
16 Gordon A L. An Antarctic oceanographic section along 170°E. Deep-

Sea Res, 1975, 22: 357–377
17 Oliver K I, Watson A J, Stevens D P. Can limited ocean mixing buffer rapid climate change? Tellus A, 2005, 57: 676–690
18 Haney R L. Surface thermal boundary conditions for ocean circulation models. J Phys Oceanogr, 1971, 1: 241–248
19 Nunes F, Norris R D. Abrupt reversal in ocean overturning during the Palaeocene/Eocene warm period. Nature, 2006, 439: 60–63
20 Zhang Z S, Wang H J, Guo Z T. Transition of thermohaline circulation modes and its impact on Cenozoic climate (in Chinese). Quat Sci, 2009, 29: 1064–1070
21 Kuhlbrodt T, Griesel A, Montoya M, et al. On the driving processes of the Atlantic meridional overturning circulation. Rev Geophys, 2007, 45: RG2001, doi: 10.1029/2004RG000166
22 Guan Y P, Huang R X. Stommel's box model of thermohaline circulation revisited—The role of mechanical energy supporting mixing and the wind-driven gyration. J Phys Oceanogr, 2008, 38: 909–917
23 Greatbatch R J, Lu J. Reconciling the Stommel box model with the Stommel-Arons model: A possible role for southern hemisphere wind forcing? J Phys Oceanogr, 2003, 33: 1618–1632
24 Toggweiler J R, Samuels B. Is the magnitude of the deep outflow from the Atlantic Ocean actually governed by Southern Hemisphere winds? In: Martin H, ed. The Global Carbon Cycle. Berlin: Springer, 1993. 303–331
25 Toggweiler J R, Samuels B. Effect of Drake Passage on the global thermohaline circulation. Deep-Sea Res I, 1995, 42: 477–500
26 Nof D. Does the wind control the import and export of the South Atlantic? J Phys Oceanogr, 2000, 30: 2650–2667
27 Olbers D, Borowski D, Völker C, et al. The dynamical balance, transport and circulation of the Antarctic Circumpolar Current. Antarct Sci, 2004, 16: 439–470
28 Sijp W P, England M H. Role of the Drake Passage in controlling the stability of the ocean's thermohaline circulation. J Clim, 2005, 18: 1957–1966
29 Broecker W S. The great ocean conveyor. Oceanography, 1991, 4: 79–89
30 Bjornsson H, Toggweiler J R. The climatic influence of Drake Passage. In: Seidov D, Haupt B J, Maslin M, eds. The Oceans and Rapid Climate Change: Past, Present and Future. Geophys Monogr Ser, 2001, 126: 243–259